## Title

Discovery and Characterization of Gut Microbiota Decarboxylases that Can Produce the Neurotransmitter Tryptamine



## Journal

Cell Host & Microbe, 16(4)

## ISSN

1931-3128

## Authors

Williams, Brianna B
Van Benschoten, Andrew H
Cimermancic, Peter
et al.

## Publication Date

2014-10-01

## DOI

10.1016/j.chom.2014.09.001

Peer reviewed

Published in final edited form as:
*Cell Host Microbe*. 2014 October 8; 16(4): 495–503. doi:10.1016/j.chom.2014.09.001.

# Discovery and characterization of gut microbiota decarboxylases that can produce the neurotransmitter tryptamine

**Brianna B. Williams**[1], **Andrew H. Van Benschoten**[1], **Peter Cimermancic**[1], **Mohamed S. Donia**[1], **Michael Zimmermann**[2], **Mao Taketani**[1], **Atsushi Ishihara**[3], **Purna C. Kashyap**[4], **James S. Fraser**[1], and **Michael A. Fischbach**[1]

[1]Department of Bioengineering and Therapeutic Sciences and the California Institute for Quantitative Biosciences, University of California, San Francisco, San Francisco, CA 94158, USA [2]ETH Zurich, Institute of Molecular Systems Biology, Zurich 8093, Switzerland [3]Faculty of Agriculture, Tottori University, Koyama, Tottori 680-8550, Japan [4]Mayo Clinic, Rochester, MN 55905, USA

## Summary

Several recent studies describe the influence of the gut microbiota on host brain and behavior. However, the mechanisms responsible for microbiota-nervous system interactions are unknown. Using a combination of genetics, biochemistry, and crystallography, we identify and characterize two phylogenetically distinct enzymes found in the human microbiome that decarboxylate tryptophan to form the β-arylamine neurotransmitter tryptamine. Although this enzymatic activity is exceedingly rare among bacteria more broadly, analysis of the Human Microbiome Project data demonstrates that at least 10% of the human population harbors at least one bacterium encoding a tryptophan decarboxylase in their gut community. Our results uncover a previously unrecognized enzymatic activity that can give rise to host-modulatory compounds and suggests a potential direct mechanism by which gut microbiota can influence host physiology, including behavior.

### Keywords

microbiome; neurotransmitter; decarboxylase

## Introduction

It is becoming increasingly clear that the gut microbiota are important for nervous system function. In 1978, excessive levels of the intestinal hormone VIP (vasoactive intestinal peptide) were discovered in cerebrospinal fluid (Ebeid et al., 1978), establishing a connection between the gut and the brain. Over the past three decades, this relationship has expanded to include pathways in the autonomic and enteric nervous systems, the

Correspondence: Michael Fischbach, Department of Bioengineering and Therapeutic Sciences University of California, San Francisco, 1700 4th Street, Byers Hall 308C, San Francisco, CA, 94158, (415) 514-9435, fischbach@fischbachgroup.org.

neuroendocrine system, and the immune system. More recently, the ability of the intestinal microbiota to modulate host neurological activity has become a focus of investigation. A 2004 study comparing germ-free and specific-pathogen-free mice demonstrated that the microbiota are required for the development of the hypothalamic-pituitary-adrenal (HPA) system, which is important for host stress response (Sudo et al., 2004). Additional studies showed that the vagus nerve is a major communication pathway used by gut bacteria to influence neurochemistry and behavior (Bravo et al., 2011), and established a role for gut microbial colonization in modulating neuronal circuits involved in motor control and anxiety behavior (Diaz Heijtz et al., 2011). A recent paper from Mazmanian and coworkers used the maternal immune activation model of autism spectrum disorder to demonstrate a role for the microbiota in the development of autism, and implicated a microbiota-derived metabolite, 4-ethylphenylsulfate, in its pathology (Hsiao et al., 2013). While it is now firmly established that the gut microbiota influence brain and behavior, the molecular mechanisms responsible for these phenomena have only begun to be explored.

In the work reported here, we had originally intended to characterize a pathway for the reductive metabolism of aromatic amino acids by the common gut Firmicute *Clostridium sporogenes*. In the course of carrying out preliminary experiments, we made the unexpected observation that *C. sporogenes* ATCC 15579 is capable of decarboxylating tryptophan (Trp) to tryptamine (Figure 1A), an activity that is exceedingly rare among bacteria. Here, we report the discovery and characterization of the *C. sporogenes* Trp decarboxylase, along with a phylogeny-informed screen of additional decarboxylases from the gut microbiota that led us to a second, unrelated Trp decarboxylase from another gut Firmicute, *Ruminococcus gnavus*. We then explore the structural determinants of Trp selectivity in the *R. gnavus* decarboxylase, and show that at least 10% of the human population harbors one of these enzymes, opening the door to future efforts to explore their potential role in mediating a microbe-host interaction.

## Results

### *Clostridium sporogenes* decarboxylates tryptophan to tryptamine

We began with an interest in the reductive metabolism of aromatic amino acids by gut-associated species of *Clostridium*. In an effort to characterize the primary products to which tryptophan (Trp) was converted, we cultivated the common gut Firmicute *Clostridium sporogenes* ATCC 15579 in rich medium, and then transferred the cell material into minimal medium to which Trp had been added. In extracts of these cultures, reverse-phase HPLC-MS analysis revealed an unexpected conversion product that was distinct from the known products of reductive Trp metabolism, indole lactic acid and indole propionic acid (Figure 1B). Since the mass of the unknown peak corresponded to the loss of the carboxylic acid group from Trp ($[M+H]^+$ *m/z*: calculated 161.22, observed 161.12), we tested and confirmed the identity of this compound to be tryptamine by co-injection with an authentic standard and by comparison of its $^1$H NMR spectrum to that of an authentic standard (Figure S1A). Notably, the presence of tryptamine in the culture fluid of *C. sporogenes* indicated that tryptamine was not only being produced but also excreted from the cytoplasm to the extracellular space.

### Identification of CLOSPO_02083 as a Trp decarboxylase

We next set out to identify the enzyme responsible for Trp decarboxylation in *C. sporogenes* ATCC 15579. The two enzyme classes most commonly associated with amino acid decarboxylation are the pyridoxal 5'-phosphate (PLP)-dependent decarboxylases, in which the catalytic cycle begins with the covalent linkage of the substrate α-amine to PLP as a Schiff base (John, 1995; Schneider et al., 2000), and the pyruvoyl-dependent decarboxylases, in which a covalently bound pyruvoyl cofactor arises from an autocatalytic posttranslational modification (Gallagher et al., 1993; van Poelje and Snell, 1990). A computational search of the *C. sporogenes* ATCC 15579 genome sequence revealed three putative PLP-dependent decarboxylases, but no putative pyruvoyl-dependent enzymes.

None of the three genes were annotated as Trp decarboxylases; CLOSPO_02083 was predicted to be a tyrosine (Tyr) decarboxylase, while CLOSPO_03076 and CLOSPO_00504 were predicted to be glutamate decarboxylases. We began by characterizing CLOSPO_02083, hypothesizing that its annotation might be correct and Trp decarboxylation was a secondary activity, or incorrect but close, since Tyr and Trp are both aromatic amino acids. The CLOSPO_02083 gene was amplified by PCR from *C. sporogenes* genomic DNA, subcloned into the pET-28a expression vector, and heterologously overexpressed in *E. coli* BL21 (DE3) as an N-terminal $His_6$ fusion protein. CLOSPO_02083 fusion protein was purified by immobilized nickel affinity chromatography to >95% homogeneity (Figure S1B). When CLOSPO_02083 was incubated with Trp for 6 min at 37 °C, HPLC analysis of the reaction mixture revealed a new peak (Figure 2A). The identity of the corresponding compound was consistent with tryptamine by co-elution with an authentic standard.

### Kinetic analysis of CLOSPO_02083 activity with aromatic amino acid substrates

The previous result shows that CLOSPO_02083 is capable of decarboxylating Trp, but it does not rule out the possibility that one of the other aromatic amino acids is transformed more efficiently. To gain insight into the substrate selectivity of CLOSPO_02083, we measured the basic kinetic parameters for CLOSPO_02083-catalyzed decarboxylation of the aromatic amino acids Trp, Tyr, and phenylalanine (Phe). To determine $k_{cat}$ and $K_m$ for CLOSPO_02083, the concentration of the amino acid substrate was varied under initial velocity conditions (Figures 2C, S4A). Trp is a robust substrate for decarboxylation CLOSPO_02083 with a $K_m$ of 2.8 ± 0.0 mM, $K_{cat}$ of 1200 $min^{-1}$ and $K_{cat}/K_m$ of $7.3\times10^3$ $M^{-1}$ $sec^{-1}$. The activity of CLOSPO_02083 against Phe was undetectable up to 90 mM substrate (Figure S1C). Although the limited solubility of Tyr prevented us from obtaining kinetic parameters, at the highest concentration of Tyr we tested, CLOSPO_02083 was 600-fold more efficient at decarboxylating Trp (Figure S1D). Collectively, these results show that Trp is accepted more efficiently as a substrate than Phe or Tyr.

These results suggest that the database annotation of CLOSPO_02083 as a Tyr decarboxylase is incorrect. The chemical distinction between Tyr and Trp is mild, since they are both aromatic amino acids. However, the biological distinction between their decarboxylation products is sharp: tyramine stimulates a pressor response that results in an increase in blood pressure (Bianchetti et al., 1982), whereas tryptamine induces the release

of serotonin from enterochromaffin cells and stimulates GI motility (Takaki et al., 1985). Thus, a modest difference in a decarboxylase's substrate selectivity can lead to entirely distinct biological outcomes, placing a premium on biochemically characterizing the substrate selectivity of amino acid decarboxylases expressed by gut commensals.

## A phylogenetic analysis of bacterial decarboxylases to select a functionally diverse set of 15 candidate enzymes

Several other gut-associated *Clostridium spp.* harbor a homolog of CLOSPO_02083, but this enzyme does not appear to be present in other gut Firmicutes. We next asked whether there exist additional unrelated Trp decarboxylases among the human microbiota. The only putative tryptophan decarboxylases in the NCBI databases come from plant and fungal genomes, but the fact that CLOSPO_02083 was misannotated as a Tyr decarboxylase led us to hypothesize that there might be other mis- or unannotated decarboxylases encoded by the microbiota that are Trp-selective.

To select a small panel of candidate decarboxylases from the microbiota, we performed a phylogenetic analysis of bacterial decarboxylases in which protein sequences were grouped into clades in which members are predicted to share a similar (if not identical) substrate selectivity. We then chose 15 enzymes for characterization in a manner that maximized our ability to search the functional space of microbiome decarboxylases: at least one sequence from each of the largest clades and three additional sequences from smaller clades (Figure S2A). We obtained and cultivated each of the host organisms to isolate genomic DNA. The candidate decarboxylases were amplified by PCR, subcloned into the pET-28a expression vector, and heterologously overexpressed in *E. coli* BL21 as N-terminal $His_6$ fusion proteins.

## A phylogeny-informed screen for additional Trp decarboxylases from the microbiota

Since our aim was to discover Trp decarboxylases rather than to obtain kinetic parameters for each enzyme in our screening panel, we developed and employed a whole-cell assay to rapidly assess the substrate selectivity of our candidate decarboxylases. *E. coli* BL21 (DE3) harboring candidate decarboxylases in pET-28a expression vectors were cultivated in rich medium and grown to stationary phase. The cells were transferred into minimal medium containing an aromatic amino acid substrate (Trp, Tyr, or Phe), and decarboxylation was monitored by analyzing cell-free culture fluid by analytical HPLC. This assay takes advantage of the fact that β-arylamines, the products of decarboxylase activity in the *E. coli* cytoplasm, could easily be detected in the extracellular fluid of *E. coli* cultures we screened and are not produced by wild-type *E. coli*.

An important limitation of the assay is that it is qualitative; in a manner that is likely due to differences in the level of active enzyme expressed, a more robust activity in the cell-based assay did not always translate into an enzyme with more efficient kinetic parameters. Moreover, we find that the assay detects low-level activities that may not be physiologically relevant, so a positive result only indicates the possibility of an activity, and must be confirmed biochemically.

Nevertheless, our qualitative assay enabled us to rapidly screen 15 decarboxylases against three substrates (Figure S2B). One of the enzymes we screened, RUMGNA_01526, appeared to be capable of decarboxylating Trp robustly; notably, this enzyme was only very distantly related to CLOSPO_02083 (26% amino acid sequence identity). To confirm this result biochemically, we purified RUMGNA_01526 fusion protein by immobilized nickel affinity chromatography to >95% homogeneity (Figure S1B).

## RUMGNA_01526 is a Trp decarboxylase

We measured the basic kinetic parameters for the decarboxylation of Trp, Tyr, and Phe by RUMGNA_01526. As shown in Figure 2D, Trp is a robust substrate for decarboxylation, with a $k_{cat}$ of 4400 $min^{-1}$, a $K_m$ of 1.1 ± 0.1 mM, and a $k_{cat}/K_m$ of $6.8\times10^4$ $M^{-1}$ $sec^{-1}$. In spite of the robust activity of RUMGNA_01526 against Trp, Tyr, and Phe in the cell-based assay, the catalytic efficiency of RUMGNA_01526 for Trp is >1000-fold higher than it is for Phe (Figures 2D and S4B), due to the combination of a higher $k_{cat}$ (19-fold) and a lower $K_m$ (70-fold). Although the limited solubility of Tyr prevented us from obtaining kinetic parameters, at the highest concentration of Tyr we tested, RUMGNA_01526 was 1000-fold more efficient at decarboxylating Trp. These data suggest that tryptophan is the native substrate of RUMGNA_01526 (Figure S1C,D).

## *R. gnavus* excretes tryptamine into the extracellular fluid

We showed above (Figure 1B) that *C. sporogenes* excretes the tryptamine generated by CLOSPO_02083 into the culture fluid. However, tryptamine produced in the cytoplasm could have a variety of alternative intracellular fates, including serving as a building block for the synthesis of a larger molecule. Having shown that RUMGNA_01526 is a Trp decarboxylase, we next asked whether *R. gnavus* excretes the tryptamine from RUMGNA_01526 into the extracellular space. We cultivated *R. gnavus* in rich medium until stationary phase, transferred the cell material into a defined medium in the absence or presence of added Trp, and monitored the extracellular fluid by analytical HPLC. We observed that after 72 hours, the concentration of tryptamine reached ~1.7 mM (Figure 2B), showing that *R. gnavus* excretes tryptamine in vitro and suggesting that this strain has the potential to excrete tryptamine in the ecological setting of the gut lumen.

## Tryptamine induces ion secretion by intestinal epithelial cells

The function of tryptamine in the context of microbe-host signaling in the gut is not well understood. As a starting point for exploring the physiology of tryptamine-mediated signaling, we performed an experiment to test whether tryptamine is capable of inducing ion secretion by intestinal epithelial cells. Using an Ussing chamber, a segment of proximal-mid murine colon was exposed to two concentrations of tryptamine and the change of short circuit current was measured. At 3 mM, a concentration comparable to the active concentration of other bacterial fermentation products such as short-chain fatty acids, tryptamine induced a significant change in short circuit current, confirming that it can affect colonic ion secretion (Figure S5). Since colonic ion secretion plays an important role in gastrointestinal motility, this result suggests that tryptamine-mediated signaling might affect the transit of food particles and bacterial cells through the gut lumen.

### RUMGNA_01526 is a fold type I PLP-dependent decarboxylase

We decided to use a combination of structural biology and phylogenetics to better understand the provenance of bacterial Trp decarboxylases. Crystals of CLOSPO_02083 in the apo form failed to diffract to an adequate resolution, but we determined the crystal structure of RUMGNA_01526 at 2.8 Å. The enzyme forms a dimer with 4565 $Å^2$ buried at the dimer interface. The active site is located at the dimer interface and therefore the enzyme is only functional in the dimeric state. The monomeric unit is comprised of three domains: an N-terminal domain containing three parallel α-helices that pack against the other monomer, a large domain comprised of a nine-stranded β-sheet surrounded by nine α-helices containing the PLP-binding site, and a smaller C-terminal domain comprised of a four-strand anti-parallel β-sheet surrounded by three α-helices (Figure 3B). The structure is nearly identical to the open form of human glutamate decarboxylase (GAD65), with an overall α-carbon RMSD of 1.07Å (Fenalti et al., 2007). Similar comparisons can be made to human aromatic amino acid decarboxylase (Giardina et al., 2011) and wild boar DOPA decarboxylase (Burkhard et al., 2001), with α-carbon RMSDs of 1.21Å and 1.23Å, respectively. The agreement between these structures highlights the commonality of this enzymatic fold, even across multiple species.

### (*S*)-α-fluoromethyltryptophan is an inhibitor of RUMGNA_01526

The close structural relationship between RUMGNA_01526 and glutamate decarboxylase raises the question of how the structural scaffold of RUMGNA_01526 accommodates the large, hydrophobic substrate Trp. Since the ideal approach to answering this question would involve determining the structure of RUMGNA_01526 bound to a Trp-mimicking inhibitor, we proceeded to determine whether a previously reported inhibitor of plant Trp decarboxylase, (*S*)- α-fluoromethyltryptophan ((*S*)- α-FMT, Figure 3*A* **I**), was an inhibitor of RUMGNA_01526 (Ishihara et al., 2011).

Although mechanistic studies have not been performed to determine the mode of Trp decarboxylase inhibition by (*S*)- α-FMT, biochemical studies with a similar amino acid analog, (*S*)- α-fluoromethylhistidine ((*S*)- α-FMH), show that this inhibitor blocks histidine decarboxylase in a mechanism-dependent fashion that involves the formation of a covalent adduct between the inhibitor and PLP.

We measured the production of tryptamine by HPLC in the presence of various concentrations of inhibitor over 30 minutes, and analyzed progress curves of the reaction to assess the kinetics of inhibition. Indeed, not only for RUMGNA_01526 but also for CLOSPO_02083, we observed linear progress curves in the presence of increasing concentrations of inhibitor, consistent with covalent inhibition (Figures 4A and 4B). Despite having a comparable $K_m$ for Trp, RUMGNA_01526 has a weaker affinity for (*S*)- α-FMT than CLOSPO_02083 ($K_i$ of 178 μM vs. 0.2 μM). However, it is more rapidly inhibited ($k_{inact}$ of 1.2 $min^{-1}$ vs. 0.1 $min^{-1}$), suggesting that once the weak enzyme-inhibitor complex forms, the relative orientation of PLP and the inhibitor is conducive to covalent bond formation (Figures 4C, 4D).

The inactivation of histidine decarboxylase by (*S*)- α-FMH is initiated by substrate decarboxylation followed by the elimination of fluoride ion (Bhattacharjee and Snell, 1990; Hayashi et al., 1986). A transaldimination releases the enamine, which can react and inactivate the PLP cofactor. In order to elucidate the mechanism by which (*S*)-α-FMT inhibits RUMGNA_01526, as well as to understand how RUMGNA_01526 accommodates the large, hydrophobic substrate Trp, we sought to determine the X-ray crystal structure of the inhibitor-bound enzyme.

## A key loop gates the active site and contacts the indole side chain of the substrate Trp

We determined the crystal structure of inhibitor-bound RUMGNA_01526 at 2.8 Å. In the active site of the native enzyme, which is located in a cleft at the dimer interface, continuous electron density shows PLP covalently linked to K306 through a Schiff base. The major difference between the native and (*S*)-α-FMT-bound structures is the conformation of an extended loop (residues 337–349). The homologous loop was previously identified as a major difference between GAD65 and GAD67, where differences in conformational dynamics are thought to be responsible for auto-inactivation of GAD65 (Fenalti et al., 2007). In porcine DOPA decarboxylase, this loop was disordered in three data sets from complexes with different inhibitors, complicating structure-based drug design and an assessment of catalytic mechanisms (Burkhard et al., 2001). In contrast, we observed that when bound to PLP alone, this loop was partially disordered and the remaining ordered components jutted away from the active site, leaving the active site solvent-exposed. Upon engagement of (*S*)-α-FMT, electron density became clearer and the loop folded over the active site, excluding solvent and forming critical interactions with the inhibitor (Figure 3D). These data are consistent with a model in which loop 337–349 gates the active site, adopting a partially disordered, outward-facing conformation in the absence of substrate that enables access to the active site, and closing down to cap the active site after substrate entry.

Two other flexible loops within the active site of the inhibitor-bound enzyme are reordered to accommodate the indole side chain of (*S*)-α-FMT. In the absence of substrate, the first loop (residues 95–101) leaves the active site accessible for the entry of a substrate with a large aromatic side chain. Upon substrate binding, the loop conformational change places the phenyl ring of Phe98 directly above the π-system of the indole ring, stabilizing the inhibitor through a π-stacking interaction (Figure 3C). This loop appears to be a critical element for defining substrate selectivity; consistent with this possibility, it is conserved among decarboxylases in several related Firmicutes (discussed below). The second loop, residues 329–336, reorients to shift the phenolic side chain of Tyr335 closer to the active site, increasing the hydrophobicity of the substrate-binding pocket.

## Insights into the mechanism of inhibition by (*S*)-α-FMT and a potential allosteric site

In the inhibitor-bound structure, (*S*)-α-FMT has been decarboxylated; however, it has not been defluorinated as seen in the mechanism of (*S*)-α-FMH inhibition of histidine decarboxylase, and remains covalently linked to PLP. This is supported by the absence of a suitable nucleophile in the active site that could be covalently modified by the defluorinated (*S*)-α-FMT-PLP adduct.

The (*S*)-α-FMT-PLP adduct (Fig 3A, **III**) is relatively disordered in the electron density maps of both active sites; however, the maps show an absence of density consistent with a covalent linkage between PLP and the enzyme. To further probe the identity of the adduct, we denatured the enzyme after incubation with PLP and (*S*)-α-FMT and analyzed the released product (Figure S10). We found a single de novo species of mass 403, which most likely represents the ketone formed after (*S*)-α-FMT is decarboxylated, defluorinated, and deaminated (Figure S10, **IV**). The same adduct is also found during the inactivation of histidine decarboxylase by (*S*)-α-fluoromethylhistidine (Bhattacharjee, M.K., and Snell, E.E.). Collectively, these data indicate that the PLP-(*S*)-α-FMT adduct is formed and remains tightly bound rather than diffusing out of the active site. Thus, the blockade of RUMGNA_01526 by (*S*)-α-FMT appears to be an enzyme-catalyzed inactivation of the PLP coenzyme, and does not involve a chemical modification of the enzyme itself.

Surprisingly, we observed an additional molecule of (*S*)-α-FMT bound to a site ~20 Å from the active site (Figure S4C). The inhibitor fits inside a hydrophobic pocket that is formed by the movement of an N-terminal loop (residues 16–22) and makes hydrogen bonds to S105 and the backbone of P102. While this binding event might be a crystallization artifact, the kinetic data are consistent with the possibility of cooperative substrate binding to an allosteric site as evidenced by a slight increase in the $r^2$ value for the fit to the Hill equation (Hill coefficient = 1.87) versus the Michaelis-Menten equation (Figure S4A, B).

## Evolutionary insights from sequence and structure into the substrate selectivity and origins of bacterial Trp decarboxylases

To better understand the mechanisms underlying the substrate recognition and specificity, we next aligned the amino acid sequences of 21 enzymes: 15 decarboxylases from the phylogeny-informed screen, three annotated histidine decarboxylases, and three decarboxylases with known structure. Three notable patterns are apparent from the multiple sequence alignment: First, while the multiple sequence alignment shows a high degree of similarity between the amino-acid substrate binding sites of the glutamate decarboxylases, the binding sites that accommodate aromatic amino-acid substrates differ significantly (Figure 5). With the exception of one enzyme (EEB27310), the only residue shared by all the sequences is K306, the active site lysine residue involved in binding PLP. Second, no apparent rules were found in the sequence alignment of the decarboxylases with aromatic amino acids as substrates that could explain their specificities or promiscuities for the aromatic amino acids; therefore, it is likely that the aromatic amino acid substrate specificity is governed by differences in the active site structures and/or orientations of the substrates. Even the serine residue at position 356 (354 in the original sequence) that was found to determine the histidine specificity of the human histidine decarboxylase (Komori et al., 2012) is found in other decarboxylases with no observed histidine activity (data not shown). Third, the binding sites of decarboxylases with aromatic amino acid substrates are rich in proline residues, suggesting that the specificity for different aromatic amino acid substrates could also be driven by active sites whose shapes match more rigidly those of the substrates.

### Trp decarboxylases are present in at least 10% of the samples from the NIH Human Microbiome Project (HMP)

Initial assemblies of sequenced human stool samples from 86 healthy subjects were examined for the presence of similar amino acid decarboxylases. We used BLASTP to search the metagenomic contigs for homologs of RUMGNA_01526. In total, we identified homologs of RUMGNA_01526 in 15 subjects (17% of the samples). Of those, 13 subjects contained only one decarboxylase homolog, while two subjects harbored two different homologs. Eight subjects (9.3%) contained a Trp decarboxylase homolog that is almost identical to the RUMGNA_01526 characterized here (>99% identical at the amino acid level over >100 residues). The rest of the samples harbored decarboxylase homologs that were 62–93% identical to RUMGNA_01526 over >100 residues (Figure 6). Although further biochemical characterization is needed to assign these more distantly related homologs as aromatic amino acid decarboxylases, a sequence alignment to RUMGNA_01526 shows nearly 100% identity over the residues critical for accepting tryptophan (Figure 6). These homologs were highly similar to genes from a variety of anaerobic Firmicute reference genomes, such as *Clostridium asparagiforme*, *Clostridium nexile*, *Desulfitobacterium dehalogenans*, and *Blautia hansenii*. Despite the fact that *C. sporogenes* ATCC 15579 is a human gut isolate, similar searches with CLOSPO_02083 yielded no hits. The presence of Trp decarboxylase homologs in 9–17% of gut metagenomes of a random population of healthy humans suggests that tryptamine produced by gut bacteria may be more prevalent in humans than previously thought.

## Discussion

The production of tryptamine by *C. sporogenes* was notable for three reasons. First, while the decarboxylation of tryptophan to tryptamine is common in the plant kingdom (Facchini et al., 2000), Trp decarboxylation is an exceedingly rare activity among bacteria. To our knowledge, the only bacterial species in which this transformation is known are *Xenorhabdus nematophilus* and *Bacillus atrophaeus*, which are thought to produce tryptamine as a building block for the biosynthesis of larger natural products (Lang et al., 2008; Li et al., 1997; Proschak et al., 2011; Yuwen et al., 2013), and *Lactobacillus bulgaricus*, the only bacterial species known to excrete tryptamine (Chander et al., 1989).

Second, tryptamine is a β-arylamine neurotransmitter known to have a range of biological activities. As a trace amine found in low quantities in the brain, it is a ligand for the trace amine-associated receptors (TAARs) that potentiates the inhibitory response of cells to serotonin (Borowsky et al., 2001; Zucchi et al., 2006), as well as a ligand for the sigma-2 receptor (Fontanilla et al., 2009). Moreover, tryptamine has been observed in human and rodent feces (Anderson, 1975; Brooks et al., 1984), where it is known to induce the release of serotonin by enterochromaffin cells (Takaki et al., 1985). Fluctuations in intestinal serotonin levels are thought to modulate GI motility (Lundgren, 1998; Turvill et al., 2000), and may play a role in the pathology of inflammatory bowel diseases (Bischoff et al., 2009; Linden et al., 2003; Linden et al., 2005). These findings are especially interesting in light of the critical role serotonin plays as a signaling molecule in the enteric nervous system (Mayer, 2011; Ormsbee and Fondacaro, 1985), where modulation of the serotonin receptors

has been proposed as a treatment for irritable bowel syndrome (Gershon and Tack, 2007; Mawe et al., 2006). Indeed, the gut microbiome of IBS patients is often dominated by Firmicutes (Jeffery et al., 2012), the phylym from which the decarboxylases described here derive, raising the question of whether the bacterial production of tryptamine plays a role in the pathogenesis of IBS.

Third, tryptamine production represents a microbiota-mediated alteration in tryptophan metabolism. Host serotonin is produced from dietary tryptophan and metabolomic profiling has shown that germ-free mice have a 2.8-fold increase in plasma serotonin over conventionalized mice, and elevated levels of tryptophan. Additionally, the level of tryptamine in feces increases by 200% in conventional verus germ free mice (Marcobal et al, 2013) and there exist microbiota-derived tryptophan metabolites such as indole propionic acid in conventionalized but not germ-free mice (Wikoff et al., 2009). Two additional reports have shown that germ-free mice have elevated levels of serotonin, 5-HT, and tryptophan (Clarke et al., 2013; Diaz Heijtz et al., 2011) without explanatory changes in gene expression of tryptophan-utilizing enzymes, and suggest that the microbiota are participating in tryptophan metabolism. Our discovery of tryptophan decarboxylases in the intestinal microbiota raises the possibility that microbes can sequester tryptophan from the diet, convert it to tryptamine, and thereby alter the spectrum and distribution of tryptophan metabolites that result in the host. Reducing the level of plasma tryptophan would decrease the production of serotonin in the brain, and could represent one mechanism by which the microbiota influence behavior.

## Materials and Methods

### Bacterial growth conditions

*Clostridium sporogenes* ATCC 15579 was grown in Reinforced Clostridium Medium (BD) supplemented with MEM Vitamins (Gibco) and incubated anaerobically at 37°C. *Ruminococcus gnavus* ATCC 29149 was grown in Brain Heart Infusion medium (BD) supplemented with yeast extract (5 g/L) and hemin (5 g/L) and incubated anaerobically at 37°C. For the qualitative cell-based decarboxylation assay, cultures were grown to stationary phase in rich medium, and the cell mass was transferred to a minimal medium (Bell, 1976) containing 5 g/L tryptophan, tyrosine, or phenylalanine. Cultures were incubated at 37°C for 24–72 h before analysis of the culture fluid by HPLC.

### Expression and purification of CLOSPO_02083 and RUMGNA_01526

Expression constructs were transformed into *E. coli* BL21 (DE3) cells, grown to saturation in LB medium (Fisher Scientific) supplemented with kanamycin (50 μg/ml) at 37°C, and diluted 1:33 into the same medium. The expression of RUMGNA_01526 N-terminal $His_6$ fusion proteins was induced at $OD_{600}$ 0.6 with 1 mM isopropyl β-D-thiogalactopyranoside, and overexpression was allowed to proceed at 25°C for 16–20 h. Cells from 1 L of culture were pelleted by centrifugation (10 min at 5,200 × *g*), resuspended in 40 ml of buffer A (300 mM NaCl, 50 mM $NaH_2PO_4$, 10 mM Imidazole, pH 8.0), and lysed by passage through a cell disruptor (EmulsiFlex C3, Avestin, Ottawa) at 10,000 pounds per square inch. Cell debris was removed by centrifugation (20 min at 31,000 × *g*) and the supernatant was

incubated with 1.5 ml of Ni-nitrilotriacetic acid resin (Qiagen, Valencia, CA) at 4°C for 1 h. After the unbound fraction was discarded, the resin was resuspended in 30 ml of buffer B (300 mM NaCl, 50 mM $NaH_2PO_4$, 20 mM Imidazole, pH 8.0), loaded onto a column, and washed with 60 ml of buffer B. Recombinant enzyme was eluted from the column with buffer C (300 mM NaCl, 50 mM $NaH_2PO_4$, 250 mM Imidazole, pH 8.0) and dialyzed at 4°C against 4 liters of buffer D (50 mM Tris-HCL pH 7.5, 300 mM NaCl). The protein was used immediately and a fresh batch was purified for each enzymatic assay. The concentrations of purified enzyme were determined spectrophotometrically using a Coomassie Protein Assay (Thermo Fisher). The expression of CLOSPO_02083 N-terminal $His_6$ fusion proteins was performed as described except for the following: LB medium was supplemented with 10 mM tryptophan and 30 μM PLP, cultures were expressed for 16–20 h at 20°C, buffers A and D contained 30 μM PLP, and 1.0 mL of Ni-nitrilotriacetic acid resin was used.

### Qualitative cell-based assay for decarboxylase substrate selectivity

Overnight cultures of *E. coli* BL21 (DE3) expressing pET-28a-*decarboxylase* constructs were diluted (1:20) into fresh LB medium containing 50 μg/ml kanamycin and grown for 90 min at 37°C. Cells were pelleted by centrifugation and resuspended in M9 minimal medium containing 5 mg/mL of tryptophan, tyrosine, or phenylalanine and 1 mM isopropyl β-D-thiogalactopyranoside. After 24 h, 100 μl of clarified supernatant was analyzed by HPLC.

### Kinetic characterization of CLOSPO_02083 and RUMGNA_01526 activity with aromatic amino acid substrates

Reaction mixtures contained 50 mM sodium phosphate pH 6.5, 300 mM NaCl, and 40 μM PLP. Reactions were initiated by the addition of enzyme and terminated by quenching aliquots with 1 volume of MeOH and performed at 37°C. All substrates purchased from Sigma-Aldrich. More details provided in Supplementary Information.

### X-ray crystallography

Crystals of RUMGNA_01526 were grown at room temperature in hanging drops consisting of equal volumes (1 + 1 μl) of 10 mg/ml RUMGNA_01526 and a crystallization solution composed of 0.1 M Bicine pH 8.5 and 25% PEG 3350. Crystals of RUMGNA_01526 with (*S*)-α-FMT were grown at room temperature in sitting drops consisting of equal volumes of 10 mg/mL RUMGNA_01526 pre-mixed with 5 mM (*S*)-α-FMT and a crystallization solution composed of 30% ethoxyethanol, 0.1 M citrate pH 5.25, and 4% polypropylene P400.

### Structure Determination and Refinement

Crystals were flash-frozen in liquid nitrogen with 10% glycerol supplemented as a cryoprotectant. Data were collected on beamline 8.3.1 at the Advanced Light Source (Table S1). X-ray reflections were processed using xia2. All subsequent molecular replacement and structure analysis was performed using the PHENIX software suite. For the structure of RUMGNA_01526 in its native form, a molecular replacement search ensemble was created from the homologous models 2JIS, 3RBF, 4E1O, 3RCH, 2QMA and 1JS3 using Phenix.sculptor and Phenix.ensembler. The structure of RUMGNA_01526 in its native form

was used as a molecular replacement search model for the (*S*)-α-FMT-bound structure. All visualization components were performed using COOT.

### Data Deposition

Protein Data Bank: Coordinates have been deposited with accession codes 4OBU (native RUMGNA_01526) and 4OBV (RUMGNA_01526-(*S*)-α-FMT complex).

## Supplementary Material

Refer to Web version on PubMed Central for supplementary material.

## Acknowledgements

We are indebted to Justin Rettenmaier for an early computational analysis of candidate decarboxylases from *Clostridium sporogenes*, and to members of the Fischbach group for ideas and helpful discussions. This work was supported by a Fellowship for Science and Engineering from the David and Lucile Packard Foundation (MAF), Medical Research Program Grant from the W.M. Keck Foundation (MAF), DARPA award HR0011-12-C-0067 (MAF), QB3 (JSF), and NIH grants OD007290 and GM081879 (MAF) and OD009180 (JSF).

## References

Anderson GM. Quantitation of tryptophan metabolites in rat feces by thin-layer chromatography. Journal of chromatography. 1975; 105:323–328. [PubMed: 1150778]

Bell SM. Treatment with gentamicin monitored by serum antibiotic assay. The Medical journal of Australia. 1976; 2:481–484. [PubMed: 186696]

Bhattacharjee MK, Snell EE. Pyridoxal 5'-phosphate-dependent histidine decarboxylase. Mechanism of inactivation by alpha-fluoromethylhistidine. The Journal of biological chemistry. 1990; 265:6664–6668. [PubMed: 2182624]

Bianchetti MG, Minder I, Beretta-Piccoli C, Meier A, Weidmann P. Effects of tyramine on blood pressure and plasma catecholamines in normal and hypertensive subjects. Klinische Wochenschrift. 1982; 60:465–470. [PubMed: 7045511]

Bischoff SC, Mailer R, Pabst O, Weier G, Sedlik W, Li Z, Chen JJ, Murphy DL, Gershon MD. Role of serotonin in intestinal inflammation: knockout of serotonin reuptake transporter exacerbates 2,4,6-trinitrobenzene sulfonic acid colitis in mice. American journal of physiology Gastrointestinal and liver physiology. 2009; 296:G685–G695. [PubMed: 19095763]

Borowsky B, Adham N, Jones KA, Raddatz R, Artymyshyn R, Ogozalek KL, Durkin MM, Lakhlani PP, Bonini JA, Pathirana S, et al. Trace amines: identification of a family of mammalian G protein-coupled receptors. Proceedings of the National Academy of Sciences of the United States of America. 2001; 98:8966–8971. [PubMed: 11459929]

Bravo JA, Forsythe P, Chew MV, Escaravage E, Savignac HM, Dinan TG, Bienenstock J, Cryan JF. Ingestion of Lactobacillus strain regulates emotional behavior and central GABA receptor expression in a mouse via the vagus nerve. Proceedings of the National Academy of Sciences of the United States of America. 2011; 108:16050–16055. [PubMed: 21876150]

Brooks JB, Nunez-Montiel OL, Basta MT, Hierholzer JC. Studies of stools from pseudomembranous colitis, rotaviral, and other diarrheal syndromes by frequency-pulsed electron capture gas-liquid chromatography. Journal of clinical microbiology. 1984; 20:549–560. [PubMed: 6490836]

Burkhard P, Dominici P, Borri-Voltattorni C, Jansonius JN, Malashkevich VN. Structural insight into Parkinson's disease treatment from drug-inhibited DOPA decarboxylase. Nature structural biology. 2001; 8:963–967.

Chander H, Batish VK, Babu S, Singh RS. Factors affecting amine production by a selected strain of Lactobacillus bulgaricus. Journal of Food Science. 1989; 54:940–942.

Clarke G, Grenham S, Scully P, Fitzgerald P, Moloney RD, Shanahan F, Dinan TG, Cryan JF. The microbiome-gut-brain axis during early life regulates the hippocampal serotonergic system in a sex-dependent manner. Molecular psychiatry. 2013; 18:666–673. [PubMed: 22688187]

Diaz Heijtz R, Wang S, Anuar F, Qian Y, Bjorkholm B, Samuelsson A, Hibberd ML, Forssberg H, Pettersson S. Normal gut microbiota modulates brain development and behavior. Proceedings of the National Academy of Sciences of the United States of America. 2011; 108:3047–3052. [PubMed: 21282636]

Ebeid AM, Smith A, Escourrou J, Murray P, Fischer JE. Increased immunoreactive vasoactive intestinal peptide in the cerebro-spinal fluid (CSF) of dogs and monkeys in hepatic failure. The Journal of surgical research. 1978; 25:538–541. [PubMed: 102874]

Facchini PJ, Huber-Allanach KL, Tari LW. Plant aromatic L-amino acid decarboxylases: evolution, biochemistry, regulation, and metabolic engineering applications. Phytochemistry. 2000; 54:121–138. [PubMed: 10872203]

Fenalti G, Law RH, Buckle AM, Langendorf C, Tuck K, Rosado CJ, Faux NG, Mahmood K, Hampe CS, Banga JP, et al. GABA production by glutamic acid decarboxylase is regulated by a dynamic catalytic loop. Nature structural & molecular biology. 2007; 14:280–286.

Fontanilla D, Johannessen M, Hajipour AR, Cozzi NV, Jackson MB, Ruoho AE. The hallucinogen N,N-dimethyltryptamine (DMT) is an endogenous sigma-1 receptor regulator. Science. 2009; 323:934–937. [PubMed: 19213917]

Gallagher T, Rozwarski DA, Ernst SR, Hackert ML. Refined structure of the pyruvoyl-dependent histidine decarboxylase from Lactobacillus 30a. Journal of molecular biology. 1993; 230:516–528. [PubMed: 8464063]

Gershon MD, Tack J. The serotonin signaling system: from basic understanding to drug development for functional GI disorders. Gastroenterology. 2007; 132:397–414. [PubMed: 17241888]

Giardina G, Montioli R, Gianni S, Cellini B, Paiardini A, Voltattorni CB, Cutruzzola F. Open conformation of human DOPA decarboxylase reveals the mechanism of PLP addition to Group II decarboxylases. Proceedings of the National Academy of Sciences of the United States of America. 2011; 108:20514–20519. [PubMed: 22143761]

Hayashi H, Tanase S, Snell EE. Pyridoxal 5'-phosphate-dependent histidine decarboxylase. Inactivation by alpha-fluoromethylhistidine and comparative sequences at the inhibitor- and coenzyme-binding sites. The Journal of biological chemistry. 1986; 261:11003–11009. [PubMed: 3733745]

Hsiao EY, McBride SW, Hsien S, Sharon G, Hyde ER, McCue T, Codelli JA, Chow J, Reisman SE, Petrosino JF, et al. Microbiota modulate behavioral and physiological abnormalities associated with neurodevelopmental disorders. Cell. 2013; 155:1451–1463. [PubMed: 24315484]

Ishihara A, Nakao T, Mashimo Y, Murai M, Ichimaru N, Tanaka C, Nakajima H, Wakasa K, Miyagawa H. Probing the role of tryptophan-derived secondary metabolism in defense responses against Bipolaris oryzae infection in rice leaves by a suicide substrate of tryptophan decarboxylase. Phytochemistry. 2011; 72:7–13. [PubMed: 21112065]

Jeffery IB, O'Toole PW, Ohman L, Claesson MJ, Deane J, Quigley EM, Simren M. An irritable bowel syndrome subtype defined by species-specific alterations in faecal microbiota. Gut. 2012; 61:997–1006. [PubMed: 22180058]

John RA. Pyridoxal phosphate-dependent enzymes. Biochimica et biophysica acta. 1995; 1248:81–96. [PubMed: 7748903]

Komori H, Nitta Y, Ueno H, Higuchi Y. Structural study reveals that Ser-354 determines substrate specificity on human histidine decarboxylase. The Journal of biological chemistry. 2012; 287:29175–29183. [PubMed: 22767596]

Lang G, Kalvelage T, Peters A, Wiese J, Imhoff JF. Linear and cyclic peptides from the entomopathogenic bacterium Xenorhabdus nematophilus. Journal of natural products. 2008; 71:1074–1077. [PubMed: 18491867]

Li J, Chen G, Webster JM. Nematophin, a novel antimicrobial substance produced by Xenorhabdus nematophilus (Enterobactereaceae). Canadian journal of microbiology. 1997; 43:770–773. [PubMed: 9304787]

Linden DR, Chen JX, Gershon MD, Sharkey KA, Mawe GM. Serotonin availability is increased in mucosa of guinea pigs with TNBS-induced colitis. American journal of physiology Gastrointestinal and liver physiology. 2003; 285:G207–G216. [PubMed: 12646422]

Linden DR, Foley KF, McQuoid C, Simpson J, Sharkey KA, Mawe GM. Serotonin transporter function and expression are reduced in mice with TNBS-induced colitis. Neurogastroenterology and motility : the official journal of the European Gastrointestinal Motility Society. 2005; 17:565–574. [PubMed: 16078946]

Lundgren O. 5-Hydroxytryptamine, enterotoxins, and intestinal fluid secretion. Gastroenterology. 1998; 115:1009–1012. [PubMed: 9786724]

Mawe GM, Coates MD, Moses PL. Review article: intestinal serotonin signalling in irritable bowel syndrome. Alimentary pharmacology & therapeutics. 2006; 23:1067–1076. [PubMed: 16611266]

Marcobal A, Kashyap PC, Nelson TA, Aronov PA, Donia MS, Spormann A, Fischbach MA, Sonnenburg JL. A metabolomic view of how the human gut microbiota impacts the host metabolome using humanized and gnotobiotic mice. ISME J. 2013; 7:1933–1943. [PubMed: 23739052]

Mayer EA. Gut feelings: the emerging biology of gut-brain communication. Nature reviews Neuroscience. 2011; 12:453–466.

Ormsbee HS, Fondacaro JD 3rd. Action of serotonin on the gastrointestinal tract. Proceedings of the Society for Experimental Biology and Medicine Society for Experimental Biology and Medicine. 1985; 178:333–338.

Proschak A, Schultz K, Herrmann J, Dowling AJ, Brachmann AO, ffrench-Constant R, Muller R, Bode HB. Cytotoxic fatty acid amides from Xenorhabdus. Chembiochem : a European journal of chemical biology. 2011; 12:2011–2015. [PubMed: 21751325]

Schneider G, Kack H, Lindqvist Y. The manifold of vitamin B6 dependent enzymes. Structure. 2000; 8:R1–R6. [PubMed: 10673430]

Sudo N, Chida Y, Aiba Y, Sonoda J, Oyama N, Yu XN, Kubo C, Koga Y. Postnatal microbial colonization programs the hypothalamic-pituitary-adrenal system for stress response in mice. The Journal of physiology. 2004; 558:263–275. [PubMed: 15133062]

Takaki M, Mawe GM, Barasch JM, Gershon MD, Gershon MD. Physiological responses of guinea-pig myenteric neurons secondary to the release of endogenous serotonin by tryptamine. Neuroscience. 1985; 16:223–240. [PubMed: 2940472]

Turvill JL, Connor P, Farthing MJ. The inhibition of cholera toxin-induced 5-HT release by the 5-HT(3) receptor antagonist, granisetron, in the rat. British journal of pharmacology. 2000; 130:1031–1036. [PubMed: 10882387]

van Poelje PD, Snell EE. Pyruvoyl-dependent enzymes. Annual review of biochemistry. 1990; 59:29–59.

Wikoff WR, Anfora AT, Liu J, Schultz PG, Lesley SA, Peters EC, Siuzdak G. Metabolomics analysis reveals large effects of gut microflora on mammalian blood metabolites. Proceedings of the National Academy of Sciences of the United States of America. 2009; 106:3698–3703. [PubMed: 19234110]

Yuwen L, Zhang FL, Chen QH, Lin SJ, Zhao YL, Li ZY. The role of aromatic L-amino acid decarboxylase in bacillamide C biosynthesis by Bacillus atrophaeus C89. Scientific reports. 2013; 3:1753. [PubMed: 23628927]

Zucchi R, Chiellini G, Scanlan TS, Grandy DK. Trace amine-associated receptors and their ligands. British journal of pharmacology. 2006; 149:967–978. [PubMed: 17088868]

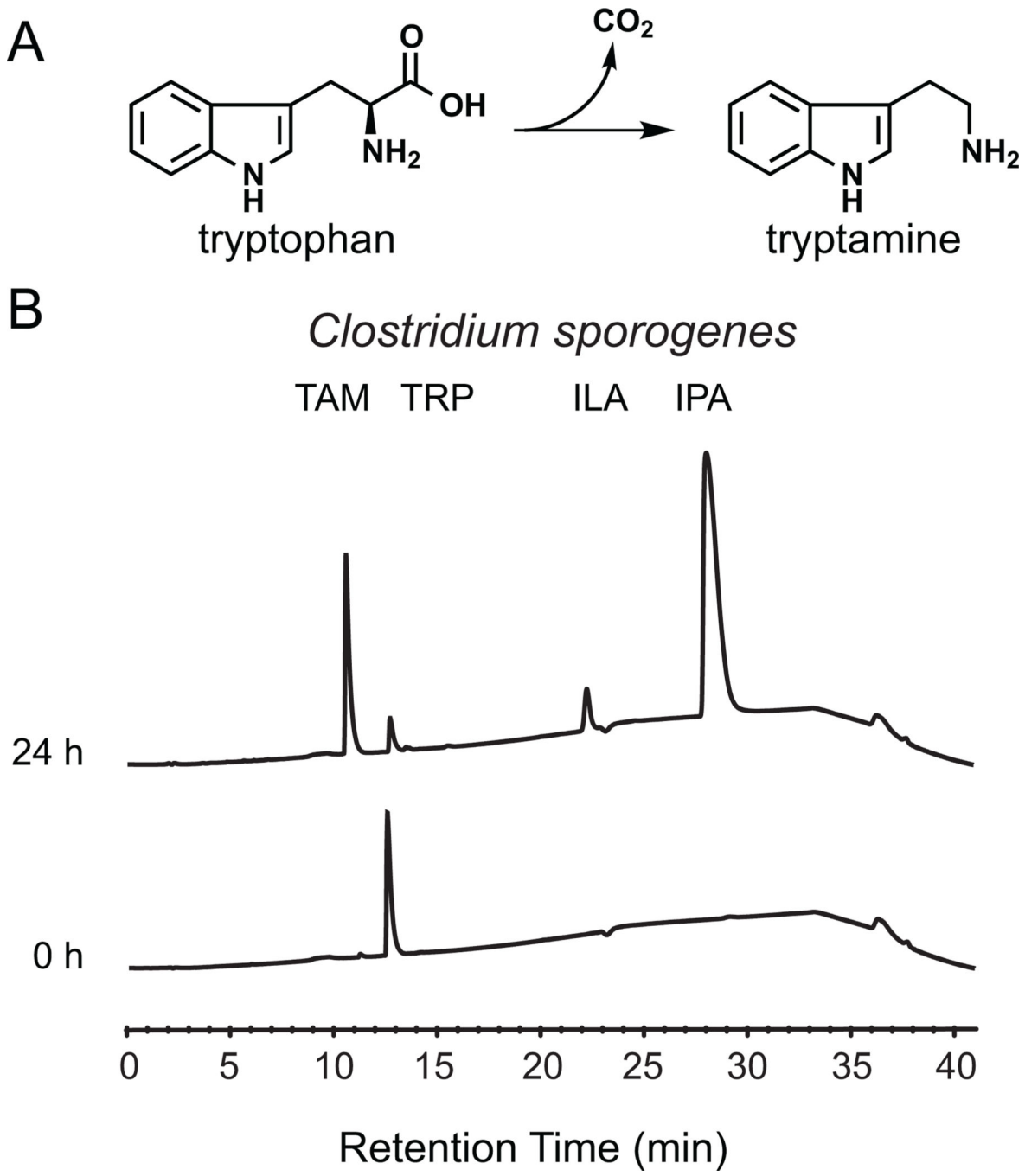


**Figure 1. Tryptamine production by *C. sporogenes***

(A) The proteinogenic amino acid L-tryptophan is decarboxylated to tryptamine, a biogenic amine neurotransmitter, by the action of pyridoxal phosphate (PLP)-dependent decarboxylases. (B) Whole *C. sporogenes* were grown anaerobically in minimal media containing 5 g/L tryptophan, and clarified supernatant was analyzed by HPLC. *C. sporogenes* converts tryptophan (12.5 min) into tryptamine (TAM, 10.5 min), indole lactic acid (ILA, 22 min), and indole propionic acid (28 min). See also Figure S1 and S5.

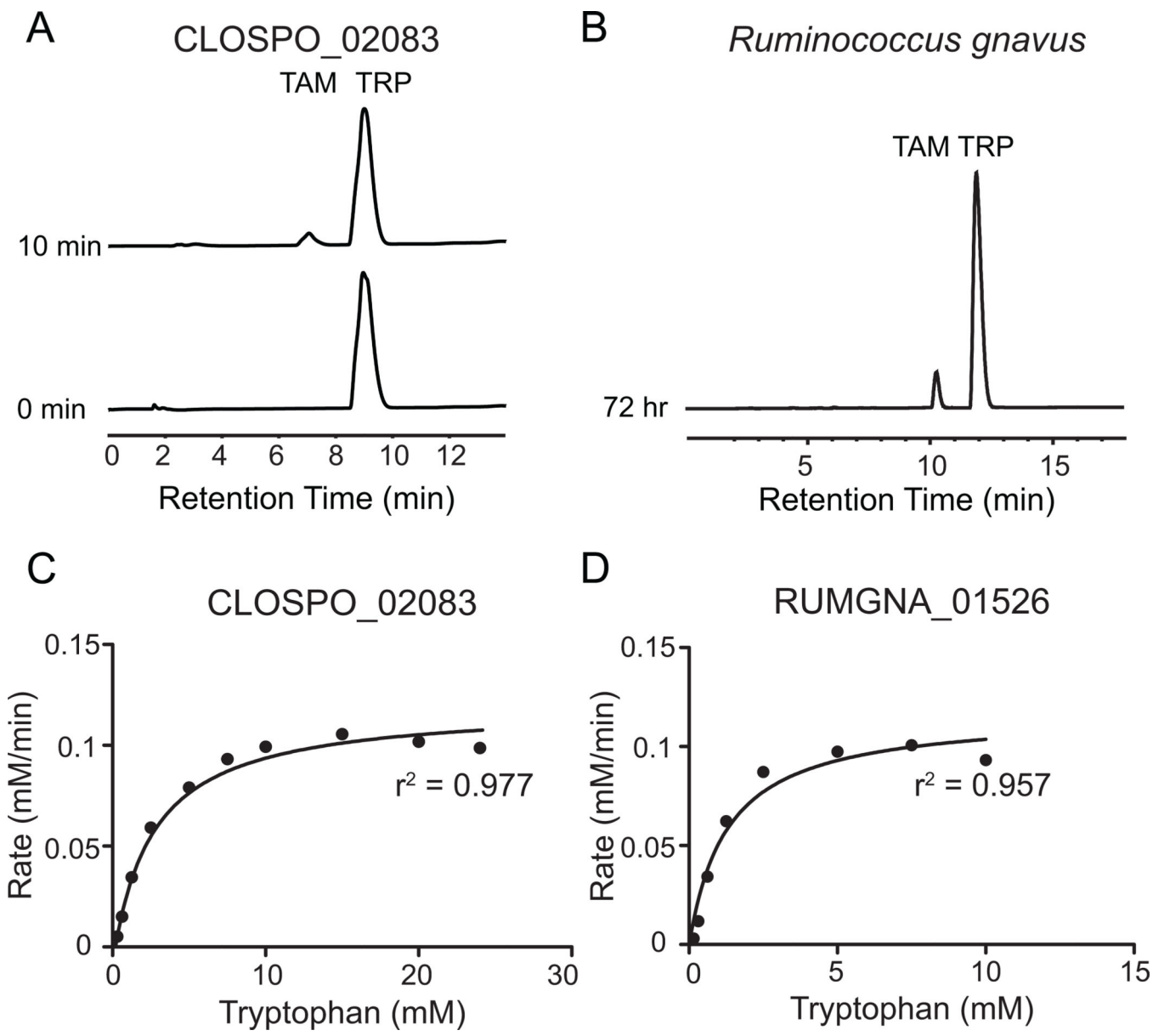


**Figure 2. CLOSPO_02083 and RUMGNA_01526 are Trp decarboxylases**

(A) 100 nM purified CLOSPO_02083 was incubated with 2.5 mM tryptophan for 10 min and quenched with 1 volume MeOH; 100 μL of the reaction mixture was analyzed by HPLC. The HPLC trace shows the conversion of tryptophan (TRP, 9 min) to tryptamine (TAM, 7 min). (B) *R. gnavus* was grown anaerobically in minimal media containing 5 g/L tryptophan; 100 μL of the clarified supernatant was analyzed by HPLC. The HPLC trace shows the conversion of tryptophan (TRP, 12.5 min) to tryptamine (TAM, 10.9 min). Note: different HPLC methods were used for 2A and 2B. (C, D) Rate (mM tryptamine/min) vs. substrate concentration curves for tryptophan decarboxylation by (C) CLOSPO_02083 or (D) RUMGNA_01526. 100 nM enzyme was incubated with concentrations of tryptophan that varied from 0.15–24.5 mM. Error represents standard error of the mean. GraphPad was

used to fit the Michaelis-Menten curve. See also Figure S2. Kinetic values are summarized in Figure S3.

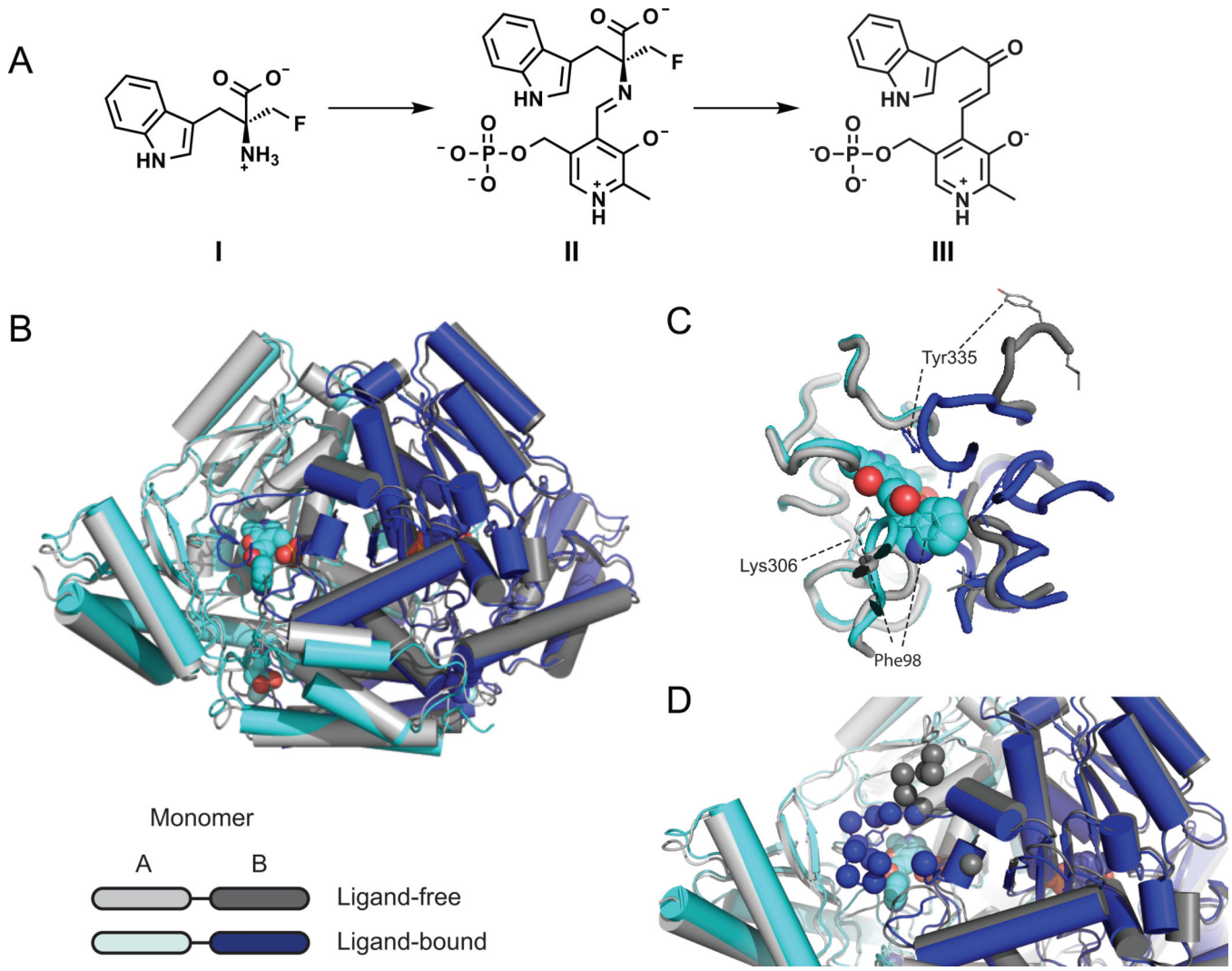


**Figure 3. Crystal structure of apo and ligand-bound RUMGNA_01526**

(A) Schematic of proposed inhibitor mechanism: (*S*)-α-FMT (**I**) is converted to a PLP-(*S*)-α-FMT external aldimine intermediate (**II**), which is decarboxylated to a PLP-(*S*)-α-FMT Schiff base adduct (**III**). (B) Overlay of ligand-free (monomer A, light gray and monomer B, dark gray) and ligand-bound (monomer A, cyan and monomer B, blue) structures. In the active and allosteric sites, PLP-(*S*)-α-FMT and (*S*)-α-FMT (respectively) are shown in spheres. (C) Active site with PLP-(*S*)-α-FMT bound reveals a repositioning of Tyr335 and Phe98. In the ligand-bound structure, Lys306 is no longer covalently bound to PLP. (D) Upon engagement of (*S*)-α-FMT, residues 337–349 (dark blue spheres) fold over the active site, excluding solvent and forming critical interactions with the inhibitor. Dark gray spheres represent only ordered residues in apo structure. See also Figure S4 and S6.

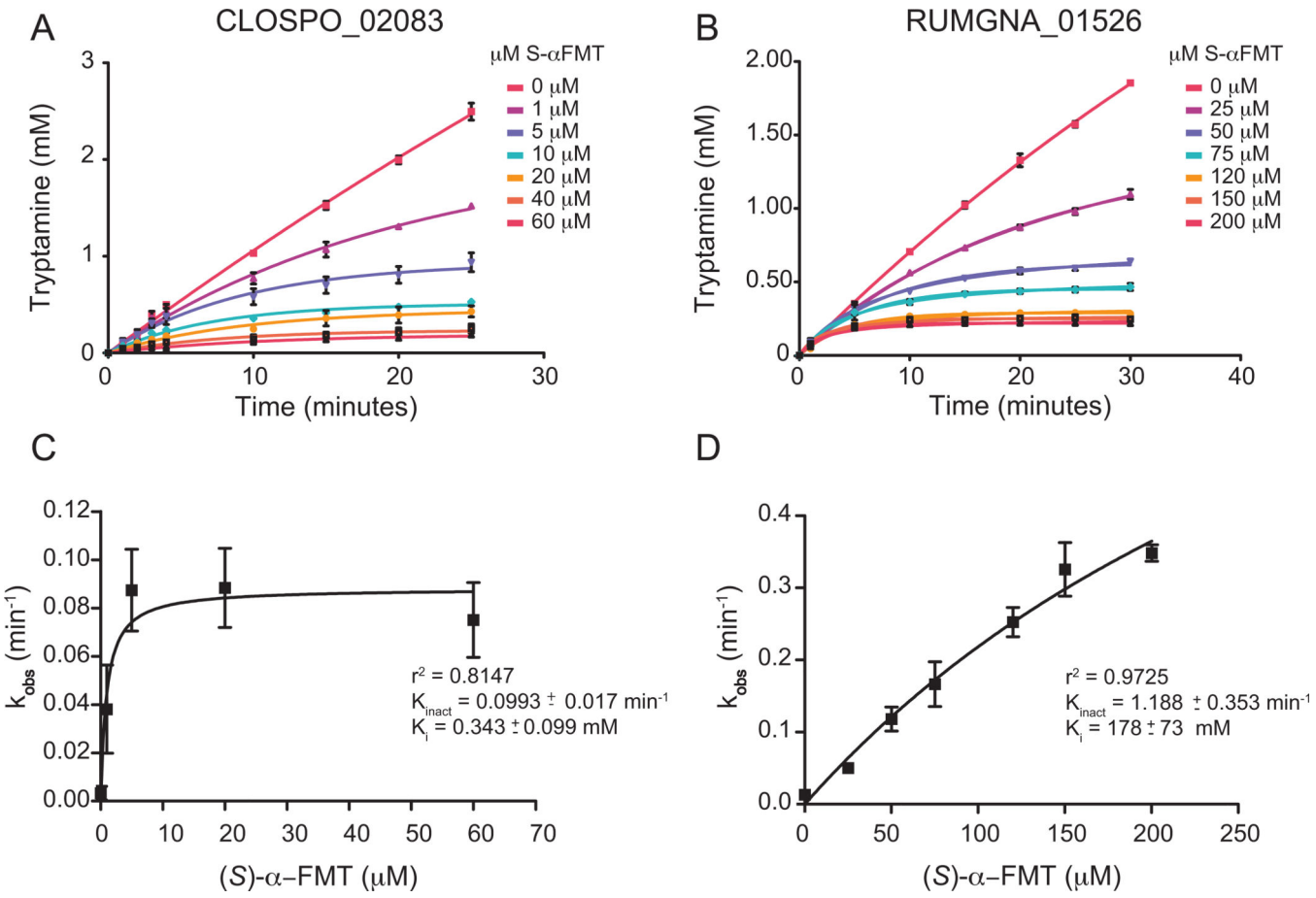


**Figure 4. Decarboxylase inhibition by (*S*)-α-FMT**

Progress curve of tryptamine production by (A) CLOSPO_02083 and (B) RUMGNA_01526 in the presence of (A) 10 mM or (B) 2.5 mM tryptophan at various concentrations of inhibitor. Data were fit to the equation described in SI Materials and Methods to obtain $k_{obs}$. (C, D) Plot of $k_{obs}$ vs [I]. CLOPSO_02083 is inhibited more potently by (*S*)-α-FMT than RUMGNA_01526 due to a higher binding affinity of the inhibitor. Error represents standard error of the mean. See also Figure S3.

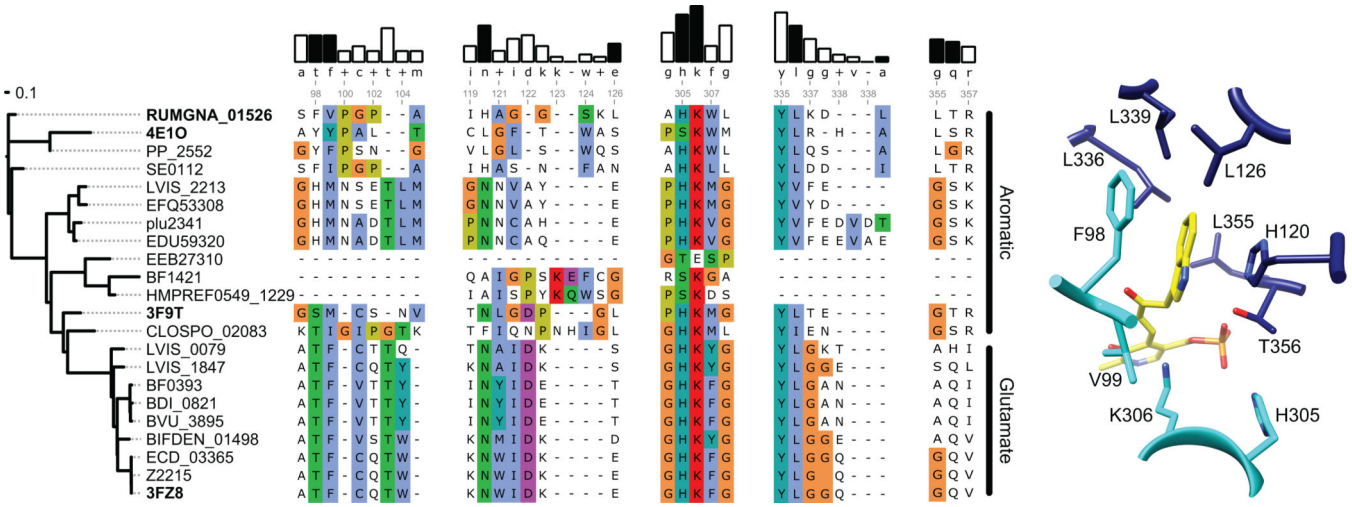


**Figure 5. Sequence and structural analysis of aromatic amino acid decarboxylases**

(A) The dendrogram on the left shows the degree of sequence similarity between various decarboxylases. (B) Alignment of select amino acid decarboxylases are numbered according to the RUMGNA_01526 sequence. Four structural components of RUMGNA_01526 important for substrate binding are highlighted. The bars above consensus sequence show the degree of sequence conservation; residues from the RUMGNA_01526 structure that interact (black bars) or do not interact (white) with the tryptophan substrate are indicated. Residues in the sequence alignment are colored according to the Clustal color code (http://ekhidna.biocenter.helsinki.fi/pfam2/clustal_colours). (C) RUMGNA_10526 active site showing residues represented by black bars in (B).

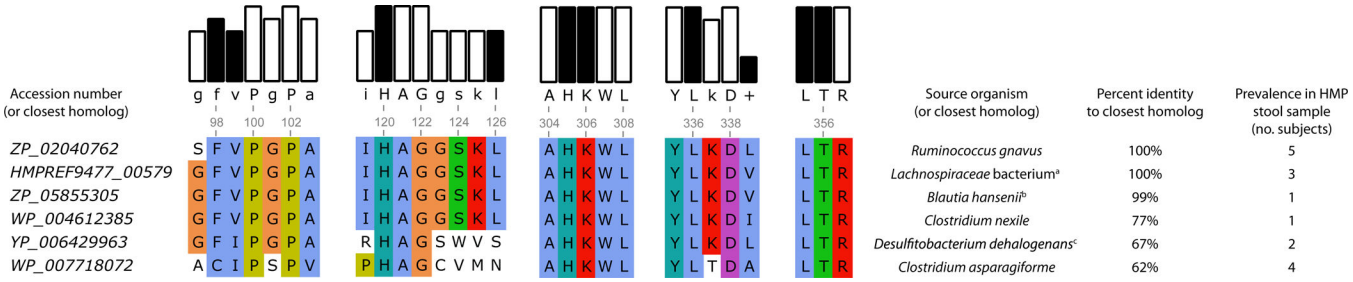


**Figure 6. Presence of tryptophan decarboxylase in the Human Microbiome Project Samples**

Accession numbers of proteins of highest sequence identity to RUMGNA_01526 (ZP_02040762). BLAST percent identity was calculated for at least 100 amino acids. 15 subjects were found to contain homologs of the putative tryptophan decarboxylases. Of those, two contained 2 different homologs, and 13 contained one homolog. One subject harbored a gene with 93% identity to either ZP_0204072 from *R. gnavus* or HMPREF9477_00579 from *Lachnospiraceae* bacterium 2_1_58FAA. A sequence alignment is presented highlighting the residues identified by our structural analysis to be important for accommodating tryptophan (black bars). (a) *Lachnospiraceae* bacterium 2_1_58FAA (b) *Blautia hansenii* DSM 20583 (c) *Desulfitobacterium dehalogenans* ATCC 51507.